FEM Thermo-Fluid Dynamic Analysis of Advanced Metal Finned Liquid Cold Plates for High Power Semiconductor Devices and Modules

Paolo Cova, Nicola Delmonte, *Senior Member, IEEE*, Davide Spaggiari, Marco Portesine, Federico Portesine, and Roberto Menozzi, *Senior Member, IEEE*

***Abstract*— This article shows two examples of finned 3-D-printable metal liquid-cooled cold plates for power semiconductor applications: a circular cold plate for press-pack devices, and a square design for power semiconductor modules. The circular cold plate for press-pack devices, fabricated by selective laser melting (SLM), is experimentally characterized and numerically simulated with a 3-D finite element method (FEM) commercial tool. The fabricated prototype shows a good geometrical definition of the fins, thanks to the optimized choice of the metal powder used by the SLM process, and of the fin block geometry. The comparison of measured and modeled temperature maps and pressure drop values also serves as validation of the FEM simulation used for the design of the rectangular cold plate for power modules. Extensive simulations are carried out in search of the optimized geometry for the rectangular fin block and the inlet and outlet terminals. The new finned 3-D-printable design for power modules is compared with a traditional serpentine design and shown to outperform it significantly in terms of both cooling efficiency and pressure drop.**

***Index Terms*— 3-D printing, cold plates, electronics cooling, finite element analysis, power electronics.**

I. Introduction and Background

POWER semiconductor devices, such as diodes, thyristors, IGBTs, and FETs, are the key components in power converters, which are becoming more and more ubiquitous, being employed in a multitude of systems and applications, including e-mobility (whether automotive, railway, nautical or avionic), industrial converters and welding systems, battery storage systems, chemical reactors, renewable energy power plants, charging stations for electrical vehicles, etc. Although these systems have now reached rather high levels of efficiency, the large amounts of power dissipated by the Joule effect over relatively small areas, hence the high power density, require high-performance optimized cooling systems to avoid overheating and consequent degradation or failure of the device and the entire system [1], [2]. In this context, liquid-cooled cold plates are typically the solution of choice, with a *coefficient of performance,* or *coefficient of operation,* defined as the ratio between the extracted power and the power spent for cooling, in the 300–500 range versus values in the 10–100 range for forced air cooling [3]. Moreover, today's metal-based additive manufacturing techniques allow the production of highly optimized designs, almost impossible to obtain with traditional milling, with a significantly improved trade-off between thermal and hydraulic performance [4], [5]. In particular, finned geometries can be achieved that have the potential to outperform standard serpentine-channel designs [5] (see also Section IV below); other, more sophisticated solutions, such as microchannels [6], are suited for integrated circuits, but as of today not for widespread industrial application to power modules and press-pack devices for reasons of cost, mechanical robustness, and manufacturing complexity; moreover, they are generally *integrated* within the device under test (DUT) rather than used to manufacture cold plates that can directly replace, with better performance, legacy products.

The design of optimized cold plates, however, is a complex task, involving the consideration of coupled thermal and hydrodynamic phenomena. Luckily, finite-element modeling (FEM) simulations have now become a very powerful, computationally efficient, and accessible tool allowing the multi-physical analysis of realistic 3-D structures directly taken from digital computer-aided design (CAD) files; once a reliable FEM model is available, sorting out different design options becomes a much quicker and less expensive process than the traditional approach of prototype fabrication and testing.

This article shows two examples of finned 3-D-printable metal liquid-cooled cold plates: a circular cold plate for press-pack devices, and a square design accommodating three power semiconductor modules; both designs are based on the same internal finned layout. The circular press-pack cold plate, a sample of which has been fabricated and characterized, was used for the validation of the FEM model, and later applied to the design of the cold plate for modules.

The article is organized as follows: Section II describes the additive manufacturing technology of choice, and the simulation tool we adopted; Section III deals with the modeling of the circular cold plate for press-pack devices, and the FEM

Manuscript received 13 April 2023; revised 15 June 2023; accepted 15 June 2023. Date of publication 23 June 2023; date of current version 20 September 2023. This work was supported in part by the Italian Ministry of Industry and Economic Development (MISE) through the Bi-Rex Competence Center under Grant 3713. Recommended for publication by Associate Editor T. Persoons upon evaluation of reviewers' comments. *(Corresponding author: Nicola Delmonte.)*

Paolo Cova, Nicola Delmonte, Davide Spaggiari, and Roberto Menozzi are with the Department of Engineering and Architecture, University of Parma, 43124 Parma, Italy (e-mail: nicola.delmonte@unipr.it).

Marco Portesine and Federico Portesine are with Poseico S.p.A., 16153 Genoa, Italy.

Color versions of one or more figures in this article are available at https://doi.org/10.1109/TCPMT.2023.3288888.

Digital Object Identifier 10.1109/TCPMT.2023.3288888

This work is licensed under a Creative Commons Attribution 4.0 License. For more information, see https://creativecommons.org/licenses/by/4.0/

model validation by comparison with experimental results; the FEM modeling approach is then applied, in Section IV, to the design of the cold plate for modules, and a few conclusions are drawn in Section V.

II. Cold Plate 3-D Printing and FEM Modeling

The cold plate designs presented in this article are based on the use of additive manufacturing, and in particular on the selective laser melting (SLM) 3-D metal printing process [7].

SLM creates the desired piece layer-by-layer, through localized fusion of the metal powder (usually a magnesium, aluminum, and silicon alloy, AlSi10Mg) by a finely tuned laser beam. The laser parameters and the optimum choice of the powder, in terms of material and particle diameter, are essential for obtaining well-defined and robust specimens [8]; robustness is key, particularly in press-pack stacks, where forces of several tens of kN can be applied to the stack [4]. Moreover, the finished printed pieces must undergo proper thermal treatments [7], [8] to avoid cracks and grain boundaries that may weaken the structure and rapidly lead to fluid leakages, and failure of the entire system. The complex machine and material parameter space generally requires computationally intensive numerical process simulations, in order to optimize the parameter values for the specific sample to be manufactured [9].

As far as the internal layout of the cold plate is concerned, previous work [4], [5] showed that finned geometries allow better thermal performance (in terms of both low thermal resistances and uniform thermal gradients) compared with that of traditional serpentine-based solutions, as well as lower pressure drop for comparable flow rates; the latter result has important consequences for the pumping apparatus, in particular in big cooling systems where several water boxes are hydraulically series-connected: relaxing the requirements on pumping power allows energy savings and reduces maintenance costs.

The modeling approach we adopted is based on 3-D FEM simulations, carried out with Comsol Multiphysics 5.3. In particular, the simulations feature full coupling between thermal and fluid dynamics equations. We used *segregated solvers* (GMRES, FGMRES), with a convergence parameter of 0.001 (i.e., the computation stops when the relative difference between the results of two successive iterations falls below 0.001). We impose the *local thermal equilibrium* condition at the sold-fluid interface. The simulation of the coolant fluid dynamics assumes laminar flow, with *no-slip* boundary condition at the interface between the cold plate internal surface and the liquid. The laminar flow assumption is supported by the Reynolds number (locally calculated by Comsol), which at 12 L/min reaches a maximum value of 2128 for the rectangular cold plate, and about 1500 for the circular one (the transition region between laminar and turbulent flow extending from 2400 to 4000); it is also worth pointing out that these peak values are attained in the inlet and outlet collectors, while the values found in the channels are much lower (<100). Pure water was considered in the model as the coolant.

For accurate solution of Navier–Stokes's and Bernoulli's equations, the tetrahedral mesh was carefully constructed for high resolution on the boundary layers, where the velocity magnitude gradient can be large. The mesh used for the rectangular cold plate described in Section IV is shown in Fig. 1; finer meshes than the one adopted in our simulations were generated to verify mesh independence of the simulation results. Adiabatic boundary conditions were applied to the symmetry planes, in order to reduce the number of degrees of freedom and, consequently, the computation time, which is typically in the order of 2 h in a 2-Xeon E5-2660 CPU workstation with 256 GB of RAM.

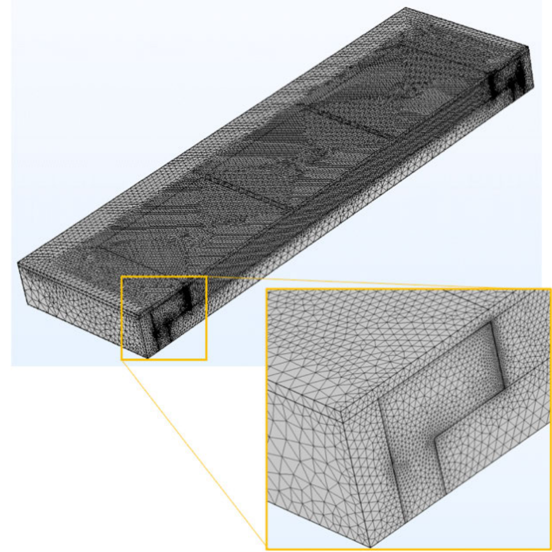

Fig. 1. Unstructured mesh used for the simulations. The inset zooms on the inlet manifold, where the boundary layer is split into two layers as is in all inner boundaries.

III. Circular Cold Plate for Press-Pack Devices

The cold plate design proposed here, a circular 14 mm thick cold plate for 48 mm diameter press-pack devices, represents the evolution of previously studied solutions [5]. The cold plate, shown in Fig. 2 together with the main model boundary conditions, is equipped with an internal finned block with uniform parallel channels, in which the coolant (filtered tap water) flows with high-velocity laminar flux; the fin thickness is 0.7 mm, the fin height is 8 mm, and the channel width is 0.5 mm (i.e., the fin pitch is 1.2 mm).

These geometrical features were found [4], [5] to offer the required cooling performance and low occurrence of channel obstructions, which tend to affect narrower channels due to incomplete powder removal at the end of the printing process, making it difficult for the SLM technique to accurately reproduce details smaller than 0.5 mm; impurities in the coolant can also contribute to obstructions in very narrow channels.

Another important point is the right choice of the diameter of the powder particles, on which the resolution of the 3-D-printed piece depends [7]. With respect to previous specimens [4], [5] the diameter of the powder grains was reduced from 50 to 30 μm, with significant improvement of the resolution of the fin block features. Combined with optimized sizing of the channel and fin size, this allowed remarkable improvement in the quality of the fabricated piece.

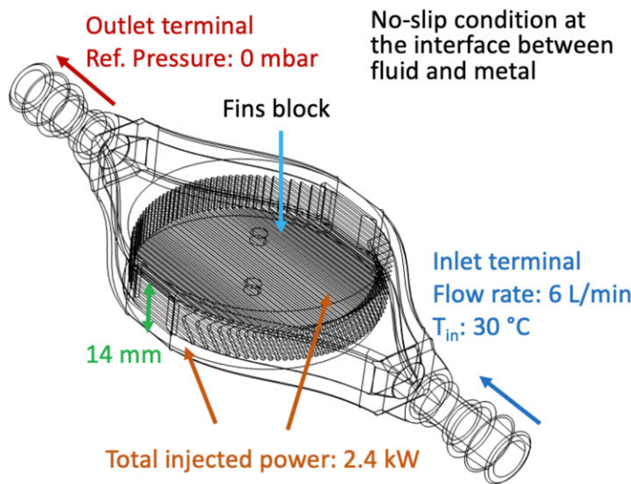

Fig. 2. Schematic representation of the external and internal geometry of the circular cold plate for press-pack devices proposed in this work; also shown are the boundary conditions used in the FEM simulations.

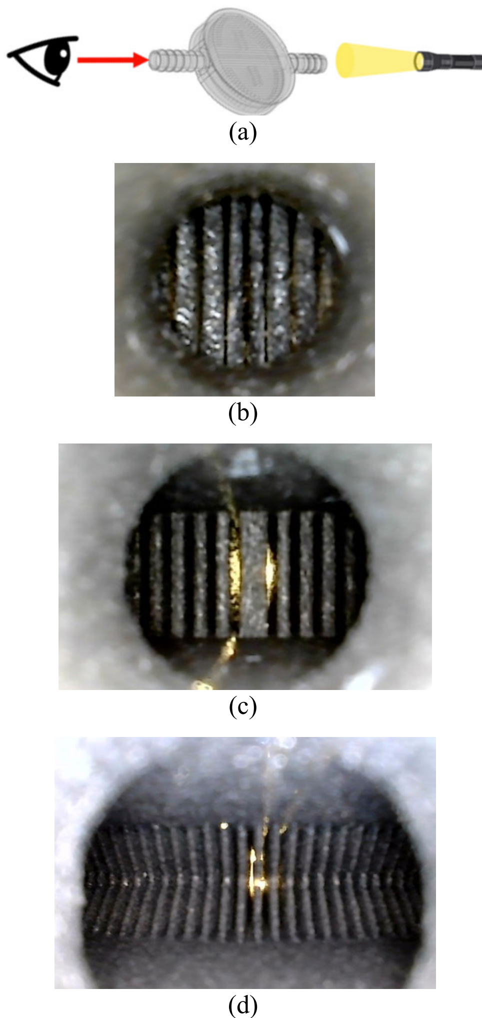

Fig. 3. Images taken at the inlet of the cold plate with an endoscopic camera: (a) imaging set-up, (b) first-generation 3-D-printed printed cold plate with obstructed channels [5], (c) second-generation 3-D-printed printed cold plate [5], and (d) third-generation 3-D-printed printed cold plate.

Fig. 3 shows a visual analysis of the internal fin block of subsequent versions of the cold plate; the images were taken using a digital endoscopic camera. As one can observe from the pictures, the more recent versions [Fig. 3(c) and (d)] show a much more regular, clean, and precise block of fins with respect to the first-generation version [Fig. 3(b)]. Optimized values of the fin geometry (0.7 mm thickness, 1.2 mm pitch) were introduced in the third-generation design [Fig. 3(d)], which was also made lighter by removing unnecessary metal from the cold plate sides and machined with lapping on the heat exchange surfaces, in order to improve the thermal contacts. Finally, starting from the second-generation version, we introduced funnel structures at the inlet and outlet terminals (Fig. 2), allowing more uniform fluid velocity distribution over the entire block of channels, hence lower thermal gradient and reduced risk of hot-spot formation.

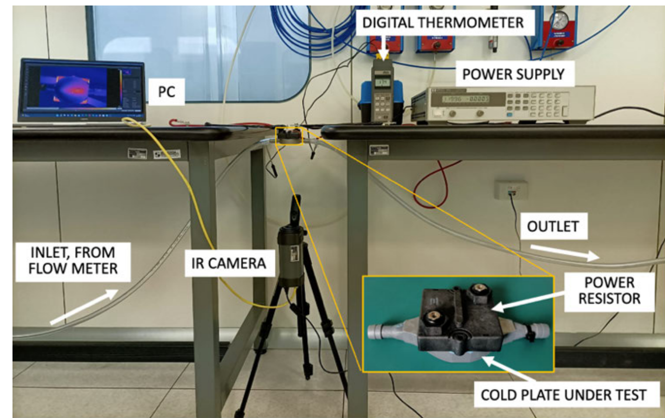

Fig. 4. Test bench view.

Temperature mapping was performed with the test bench described in [5] and shown in Fig. 4. The cold plate was heated by a 600 W, 1 Ω power resistor in thermal contact with one of its surfaces (the resistor is electrically insulated from the cold plate to avoid the risk of electrical shocks by contact with the water pipes); the corresponding unit-area power density is 17.4 W/cm^2. The contact was ensured by a layer of bicomponent adhesive thermal grease (Bergquist TGF 3600 thermal grease, with thermal conductivity of 3.6 W/m·K). The opposite cold plate surface, instead, was kept free and treated with a layer of opaque spray paint, in order to reduce reflection in the infrared band, and analyzed with a digital thermal camera; images were taken at the end of thermal transients, under steady-state conditions. The emission coefficient of the surface under test was calibrated until the temperature measured by the thermal camera under steady-state conditions was the same as the ambient temperature measured with a mercury-column thermometer. The estimated accuracy is about 0.5 °C for the thermal camera and 0.2 °C for the thermocouples. We measured the flow rate and inlet and outlet water temperatures using a rotameter and K-type thermocouples, respectively. The resistor-cold plate assembly is not insulated during the measurement; however, the injected power is calculated from the temperature difference between the outflowing and the inflowing fluid, so any power loss that there may occur does not impact the accuracy of our estimates.

Fig. 5 shows the comparison between measured (top) and simulated (bottom) thermal maps. The first point to note is the good overall agreement between measurements and

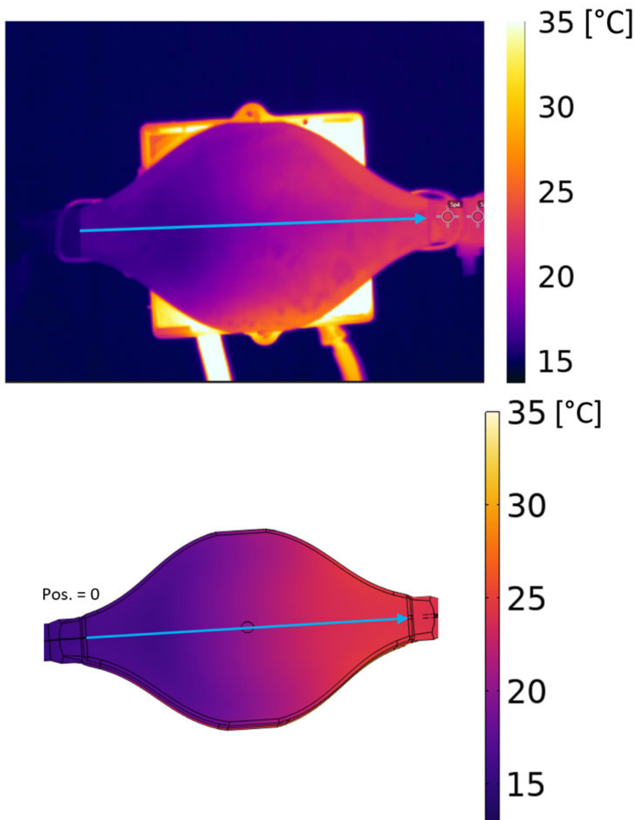

Fig. 5. Measured (top) and simulated (bottom) thermal maps. The power dissipated by the heating resistor is 520 W, and the flow rate is 1.05 L/min. The blue arrows indicate the line along which the temperature profiles of Fig. 6 are taken.

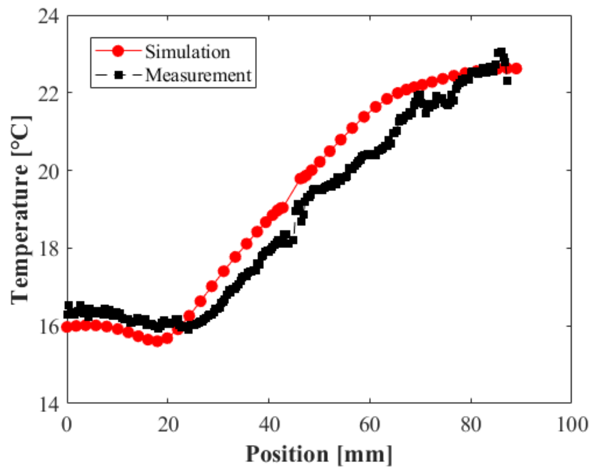

Fig. 6. Measured and simulated temperature profiles along the blue lines in Fig. 5. The dissipated power is 520 W, and the flow rate is 1.05 L/min.

model, in terms of 2-D temperature distribution and values. Second, with respect to previous results [5], no hot spots or anomalous thermal gradients are observed anywhere in the structure, thanks to the aforementioned improved design and good uniformity in the 3-D printing of the fin block.

The measured and simulated temperature profiles along the central axis of the cold plate (blue arrows in Fig. 5) can be seen in Fig. 6. While the match between the two curves is satisfactory, the experimental data indicate a slightly better performance than that predicted by the model, probably thanks to some internal surface roughness, unaccounted for in the simulations, actually increasing the heat exchange surface between water and metal.

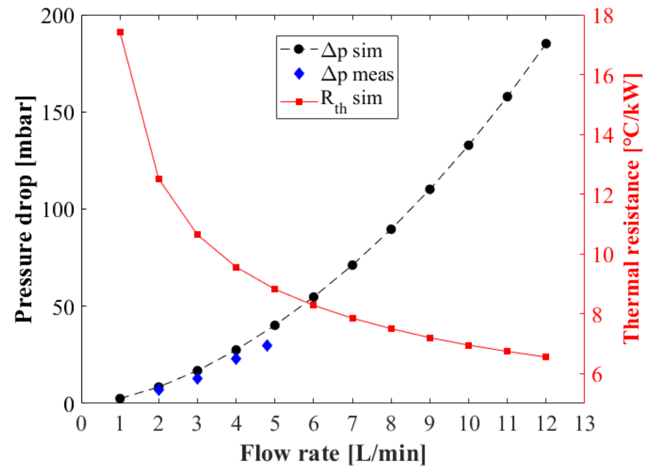

Fig. 7. Pressure drop (simulated and measured) and thermal resistance at different values of flow rate for the cold plate of Fig. 2. The injected thermal power is 2.4 kW.

The performance is improved, both in terms of thermal resistance and pressure drop, if compared with a traditional serpentine-based solution [4]. A few pressure drop values measured with a precision manometer (Fluke 700G27 300 PSIG) are included in Fig. 7 (blue diamonds). The experimental cold plate pressure drop was calculated by subtracting from the total pressure drop the parasitic series pressure drop, measured after removing the cold plate from the hydraulic circuit. The measurement range was limited by the flowmeter range (2.0–4.8 L/min). There is a slight (about 20%) deviation of the simulated values relative to the measured ones, which could be explained at least in part by some discrepancy between the actual fin geometry and the simulated one: as a matter of fact, observing the cold plate from the input terminal [Fig. 3(d)], the fins appear to be slightly thinner than the nominal value (the one set in the simulations), due to printing tolerances; this results in slightly wider channels, hence the lower measured pressure drop with respect to the simulations.

Considering the good compromise it offers between performance and manufacturability, the fin width used for the circular cold plate described so far was also adopted for the design of the rectangular cold plate for power modules that is discussed in Section IV.

IV. Rectangular Cold Plate for Power Modules

In this section, we present FEM simulations of a novel design for a finned-geometry 3-D-printable (FG3-D) rectangular cold plate for power modules. Rectangular cold plates are the standard solution for single-side cooling of power modules [10], multi-chip server modules [11], or battery packs [12], [13], [14]. This analysis is an extension of previous work [5] that showed finned layouts to outperform the traditional serpentine-geometry solutions.

In this work we consider a 20 mm thick water box; this value was shown to offer a good trade-off between pressure

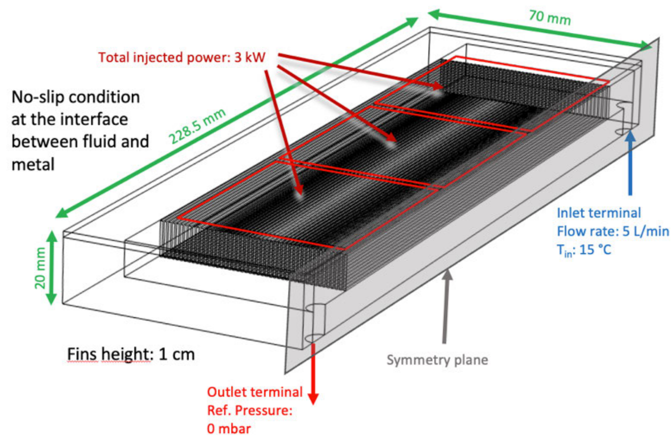

Fig. 8. Geometry details and FEM boundary conditions for the rectangular finned cold plate for power modules (case with channel width of 0.5 mm). Only half of the cold plate is shown and was simulated thanks to the symmetry plane.

TABLE I
FEM SIMULATION RESULTS FOR FINNED RECTANGULAR COLD PLATES

Flow rate [L/min]	Channel width [mm]	R_{TH} [°C/kW]	T_{ave} [°C]	T_{max} [°C]	Δp [mbar]
1	0.5	9.9	44.8	65.3	4.7
	0.7	10.6	46.9	67.7	3.3
	0.9	11.3	48.8	69.4	2.9
	1.1	11.4	49.3	68.3	2.7
3	0.5	4.6	28.9	36.3	30.8
	0.7	5.2	30.6	38.2	25.5
	0.9	5.8	32.3	40.1	23.2
	1.1	6.1	33.4	40.8	22.8
5	0.5	3.6	25.7	30.4	76.3
	0.7	4.1	27.3	32.4	67.0
	0.9	4.6	28.9	34.3	62.2
	1.1	5.0	30.0	35.3	61.8
7	0.5	3.1	24.3	27.9	140.6
	0.7	3.6	25.8	29.8	127.9
	0.9	4.1	27.4	31.7	119.8
	1.1	4.5	28.4	32.8	119.8
9	0.5	2.8	23.5	26.5	223.6
	0.7	3.3	25.0	28.4	207.9
	0.9	3.8	26.4	30.2	195.9
	1.1	4.2	27.5	31.4	196.4
11	0.5	2.6	22.9	25.6	325.5
	0.7	3.1	24.4	27.4	307.0
	0.9	3.6	25.8	29.2	290.5
	1.1	3.9	26.8	30.4	292.0

drop, thermal resistance, and cold plate volume and weight. The fin width is kept fixed at 0.7 mm (as in the circular cold plate of Section III). On the other hand, we vary the channel width between 0.5 and 1.2 mm in search of the optimum geometry of the fin block. Fig. 8 shows (half of) the FG3-D cold plate in the case of 0.5 mm wide channels, together with the main dimensional details and model boundary conditions. As indicated in the figure, the cold plate is designed to accommodate three power modules (dissipating 1 kW each in our simulations).

Table I shows some of the results of this simulation campaign: we varied the flow rate from 1 L/min to 16 L/min; however, we observed numerical convergence problems beyond 12 L/min, probably due to the onset of turbulence phenomena, so we limited the analysis to this upper bound; moreover, although we varied the flow rate with 1 L/min steps, for the sake of compactness Table I shows results with 2 L/min resolution. As can be expected the cold plate thermal resistance increases with the channel width, due to the reduction of the heat exchange surface, resulting in higher values of average (T_{ave}) and maximum (T_{max}) temperatures; on the other hand, thinner channels result in larger pressure drops for any fixed value of the water flow rate.

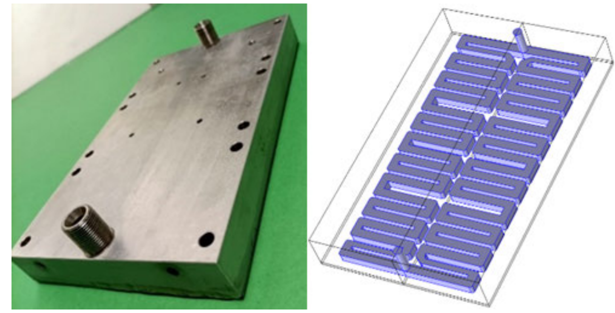

Fig. 9. External (left) and internal (right) view of the traditional, commercial serpentine cold plate (TCP) [5].

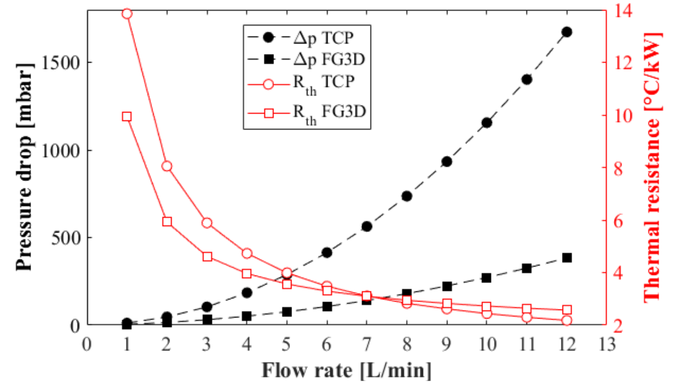

Fig. 10. Simulated pressure drop and thermal resistance comparison between the finned-geometry 3-D-printable FG3-D cold plate (channel width of 0.5 mm), and a traditional cold plate (TCP) based on serpentine geometry, as a function of the water flow rate. The total injected power is 3 kW, and the inlet water temperature is 15 °C.

However, we chose 0.5 mm for the channel width because the corresponding pressure drop values are quite acceptable for practical cooling systems, and much lower than those offered by traditional serpentine-geometry cold plates, as shown below.

In the following we compare the simulated performance of the FG3-D cold plate with that of a traditional cold plate (TCP) based on a serpentine geometry, an example of which is shown in Fig. 9. The serpentine-channel cold plate is a commercial product successfully adopted to cool power modules of the size and power rating we are considering here, hence it represents a significant benchmark for novel designs. The comparison between the novel proposed design (Fig. 8) and the traditional serpentine-channel design (Fig. 9) is made for the same heat exchange area (module area).

Fig. 10 shows the pressure drop and the thermal resistance computed in the two designs as a function of the water

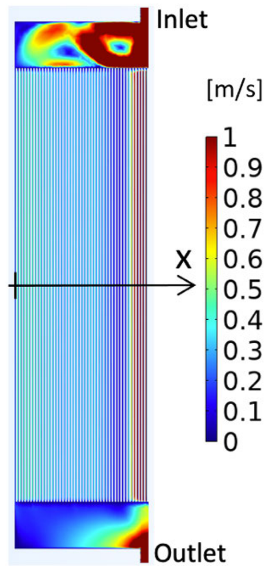

Fig. 11. Simulated water velocity magnitude map for (half of) the FG3-D cold plate with horizontal inlet/outlet terminal arrangement.

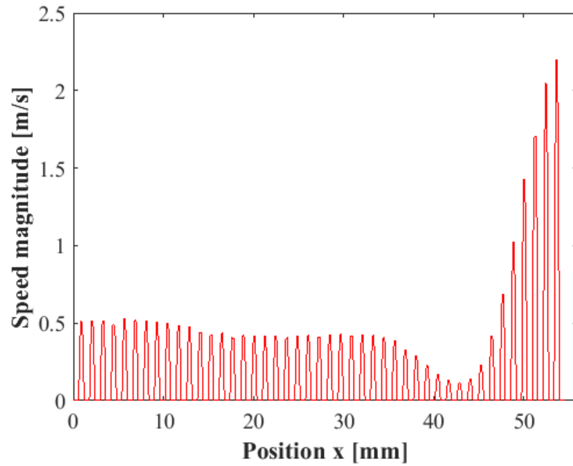

Fig. 12. Simulated water velocity magnitude for (half of) the FG3-D cold plate with horizontal inlet/outlet terminal arrangement, along the black line (x) shown in Fig. 11.

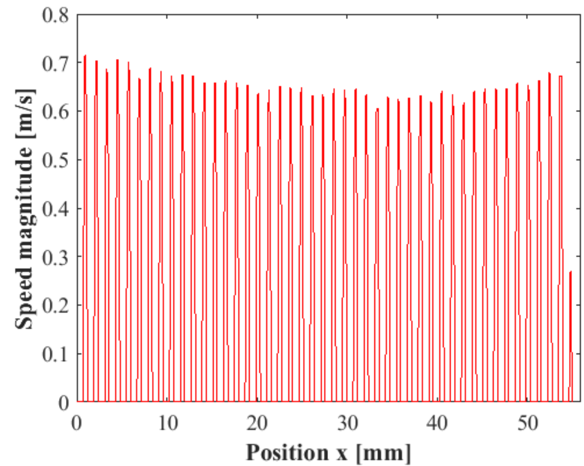

Fig. 13. Simulated water velocity magnitude for (half of) the FG3-D cold plate with vertical inlet/outlet terminal arrangement, along the black line (x) shown in Fig. 11.

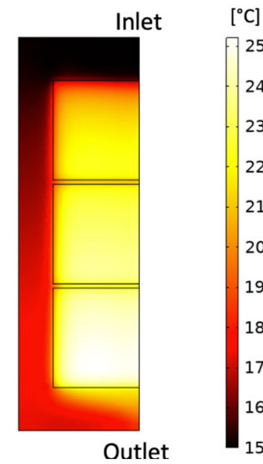

Fig. 14. Simulated thermal map of (half of) the FG3-D cold plate with vertical inlet/outlet arrangement; the channel width is 0.5 mm, the total dissipated power is 3 kW, the flow rate is 12 L/min, and the inlet water temperature is 15 °C.

flow rate. It is clearly visible how, for comparable values of the thermal resistance, the finned design outperforms the serpentine design in terms of pressure drops. The FG3-D cold plate performs better than the TCP also in terms of thermal resistance, except at the high end of the flow rate range, where the TCP cannot practically operate due to excessive pressure drop.

It is worth mentioning that one of the novel features of the FG3-D design is the presence of vertical inlet and outlet terminals (see Fig. 8). This arrangement, as opposed to the traditional horizontal inlet/outlet arrangement, offers a distinctive advantage in the hydraulic performance of the cold plate, ensuring very uniform fluid velocity distribution over all the channels. On the other hand, with a more traditional horizontal inlet/outlet arrangement, the central channels of the fin block, which are those that directly face the inlet, show a significantly higher water velocity than the peripheral ones, as shown in Figs. 11 and 12; this obviously reflects in nonuniform cooling, hence worse thermal performance. The excellent water velocity uniformity offered by the vertical inlet/outlet arrangement is clearly illustrated in Fig. 13, resulting in the very uniform temperature distribution shown by the thermal map in Fig. 14.

V. Conclusion

This article showed two examples of finned 3-D-printable metal liquid-cooled cold plates for power semiconductor applications: a circular cold plate for press-pack devices, and a square design accommodating three power semiconductor modules. The finned blocks can be fabricated by the SLM 3-D metal printing process.

The circular cold plate for press-pack devices was described in detail (also in comparison with previous less mature versions) experimentally characterized and numerically simulated with a 3-D finite element method (FEM) commercial tool. The latest prototype shows a much improved geometrical definition of the fins, thanks to the optimized choice of the metal powder used by the SLM process and of the fin block geometry, and

can now be considered a mature product, ready to be tested in a complete leg of a press-pack converter, before final market deployment.

The temperature maps and pressure drop values measured on the circular cold plate were compared with the modeled results to validate the FEM simulations that were used for the design of the rectangular cold plate for power modules.

Extensive simulations were carried out for the rectangular cold plate in search of the optimized geometry for the fin block over a wide range of cooling fluid (water) flow rates. Novel vertical inlet and outlet terminals were also compared with horizontal ones and shown to yield much improved uniformity of water velocity distribution among the parallel channels, hence better thermal performance. The new finned 3-D-printable design was compared with a traditional serpentine design and shown to outperform it significantly in terms of both cooling efficiency and pressure drop, with important implications for the cost of the hydraulic system, particularly for hydraulically series-connected cold plates.

The simulations and measurements shown in the article demonstrate the effectiveness of 3-D-printed finned liquid-cooled cold plates for high-power semiconductor applications, which, thanks to highly customizable layouts, allow very good thermal and hydraulic performance. This promises improved device reliability, thanks to lower operating temperatures and more uniform temperature distributions, as well as more efficient, cheaper, and less cumbersome hydraulic cooling systems. The use of advances 3-D printing techniques such as SLM also yields improved reliability of the cooling system itself, thanks to the absence of welded joints and gaskets, which are prone to liquid leaks possibly causing system failures.

Acknowledgment

The authors are grateful to Emilio Sacchi and Mario Aschero of Poseico for the preparation of 3-D-printed prototypes.

References

[1] S. G. Kandlikar and C. N. Hayner, "Liquid cooled cold plates for industrial high-power electronic devices—Thermal design and manufacturing considerations," *Heat Transf. Eng.*, vol. 30, no. 12, pp. 918–930, Oct. 2009, doi: 10.1080/01457630902837343.

[2] M. Lazzaroni et al., "Metrological characterization of cold plates for power converters," *IEEE Trans. Instrum. Meas.*, vol. 65, no. 1, pp. 37–45, Jan. 2016, doi: 10.1109/TIM.2015.2479104.

[3] E. Laloya, Ó. Lucía, H. Sarnago, and J. M. Burdío, "Heat management in power converters: From state of the art to future ultrahigh efficiency systems," *IEEE Trans. Power Electron.*, vol. 31, no. 11, pp. 7896–7908, Nov. 2016, doi: 10.1109/TPEL.2015.2513433.

[4] P. Cova, D. Santoro, D. Spaggiari, F. Portesine, F. Vaccaro, and N. Delmonte, "CFD modeling of additive manufacturing liquid cold plates for more reliable power press-pack assemblies," *Microelectron. Rel.*, vol. 114, Nov. 2020, Art. no. 113734, doi: 10.1016/j.microrel.2020.113734.

[5] P. Cova, N. Delmonte, D. Spaggiari, M. Portesine, F. Portesine, and R. Menozzi, "FEM analysis of 3D printable finned metal liquid cold plates for semiconductor power modules," in *Proc. 28th Int. Workshop Thermal Invest. ICs Syst. (THERMINIC)*, Dublin, Ireland, Sep. 2022, pp. 1–5, doi: 10.1109/THERMINIC57263.2022.9950670.

[6] Z. Zhang, X. Wang, and Y. Yan, "A review of the state-of-the-art in electronic cooling," *e-Prime Adv. Electr. Eng., Electron. Energy*, vol. 1, 2021, Art. no. 100009, doi: 10.1016/j.prime.2021.100009.

[7] W. E. Frazier, "Metal additive manufacturing: A review," *J. Mater. Eng. Perform.*, vol. 23, no. 6, pp. 1917–1928, Jun. 2014, doi: 10.1007/s11665-014-0958-z.

[8] S. L. Lin, C. C. Lin, D. Y. Lin, and C. S. Chuang, "Laser additive manufacturing technology in titanium 64 implant of microstructure fabrication and analysis," in *Proc. 8th Annu. IEEE Int. Conf. Nano/Micro Engineered Mol. Syst.*, Suzhou, China, Apr. 2013, pp. 594–597, doi: 10.1109/NEMS.2013.6559801.

[9] K. K. Fletcher, T. E. Sparks, A. Flood, and F. Liou, "A SOA approach to improve performance of metal additive manufacturing simulation," in *Proc. IEEE Int. Conf. Cognit. Comput. (ICCC)*, Honolulu, HI, USA, Jun. 2017, pp. 140–143, doi: 10.1109/IEEE.ICCC.2017.26.

[10] D. Karimi, H. Behi, J. Jaguemont, M. El Baghdadi, J. Van Mierlo, and O. Hegazy, "Thermal concept design of MOSFET power modules in inverter subsystems for electric vehicles," in *Proc. 9th Int. Conf. Power Energy Syst. (ICPES)*, Perth, WA, Australia, Dec. 2019, pp. 1–6, doi: 10.1109/ICPES47639.2019.9105437.

[11] B. Ramakrishnan et al., "Experimental characterization of cold plates used in cooling multi chip server modules (MCM)," in *Proc. 17th IEEE Intersociety Conf. Thermal Thermomechanical Phenomena Electron. Syst. (ITherm)*, San Diego, CA, USA, May 2018, pp. 664–672, doi: 10.1109/ITHERM.2018.8419643.

[12] S. Panchal, R. Khasow, I. Dincer, M. Agelin-Chaab, R. Fraser, and M. Fowler, "Thermal design and simulation of mini-channel cold plate for water cooled large sized prismatic lithium-ion battery," *Appl. Thermal Eng.*, vol. 122, pp. 80–90, Jul. 2017, doi: 10.1016/j.applthermaleng.2017.05.010.

[13] B. Xia et al., "Thermal analysis and improvements of the power battery pack with liquid cooling for electric vehicles," *Energies*, vol. 12, no. 16, p. 3045, Aug. 2019, doi: 10.3390/en12163045.

[14] K. Benabdelaziz, B. Lebrouhi, A. Maftah, and M. Maaroufi, "Novel external cooling solution for electric vehicle battery pack," *Energy Rep.*, vol. 6, pp. 262–272, Feb. 2020, doi: 10.1016/j.egyr.2019.10.043.

Paolo Cova was born in Milan, Italy, in 1966. He received the Laurea degree in electronics engineering and the Ph.D. degree in information technology from the University of Parma, Parma, Italy, in 1992 and 1996, respectively.

Since 1992, he has been with the University of Parma, where he has been an Assistant Professor, since 2000, and an Associate Professor, since 2019. He has authored more than 180 scientific papers in international journals or international conference proceedings. His research activities have covered characterization and reliability evaluation of electronic and optoelectronic III–V compound semiconductor devices, thermal modeling and reliability of power devices and converters.

Prof. Cova is associated with the Italian Institute of Nuclear Physics (INFN) for thermal studies of power converters for high energy physics experiments at CERN and a member of the Dune Collaboration. He is an Associate Editor of Microelectronics Reliability and a TPC Member of the European Conference on Reliability of Electron Devices (ESREF).

Nicola Delmonte (Senior Member, IEEE) was born in Manfredonia, Italy, in 1967. He received the Laurea degree in electronic engineering and the Ph.D. degree in information technology from the University of Parma, Parma, Italy, in 2002 and 2006, respectively.

Since 2002, he has been with the Department of Engineering and Architecture, University of Parma, where he became a Research Fellow, in 2005, an Assistant Professor, in 2013, and an Associate Professor, in 2018. His current research interests include the electrical and thermal characterization, modeling, reliability evaluation of power devices and hybrid modules, design of renewable-energy plants, nanogrids, and smart systems.

Davide Spaggiari was born in Parma, Italy, in 1995. He received the master's degree (cum laude) in electronic engineering from the University of Parma, Parma, in 2020, where he is currently pursuing the Ph.D. degree.

His research activity mainly focuses on the design through FEM simulations of metal liquid heat sinks for semiconductor power devices (press-pack and modules). Other projects include FEM simulations of high-frequency transformers and the development of resistive tomography systems for groundwater monitoring.

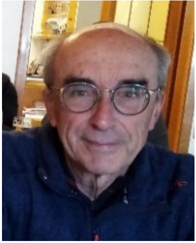

Marco Portesine was born in Genoa, Italy, in 1954. He received the Laurea degree in electronic engineering from the University of Genoa, Genoa, in 1978.

He is the Manager of Research and Development activities and the CEO of Poseico, Genoa. He has been active in power semiconductors and power electronics research and development for over 45 years and has collaborated with major European and international power electronic companies and research laboratories on publicly and privately funded research projects. He has authored or coauthored 47 scientific papers published in international journals or international conference proceedings. His research interests include electrical, physical characterization, and development of new power devices, manufacturing processes and cooling systems for MW-scale power electronics.

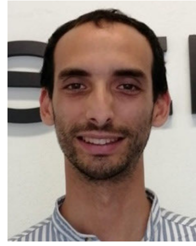

Federico Portesine was born in Genoa, Italy, in 1992. He received the Laurea degree in electric engineering from the University of Genoa, in 2018.

Since 2017, he has been with Poseico as a Power Semiconductor and Production Engineer. He manages Poseico's power semiconductors production line and the development of new products, including water-cooled heatsinks for power converter applications.

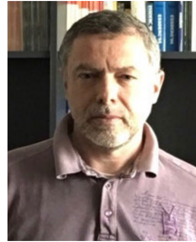

Roberto Menozzi (Senior Member, IEEE) received the Laurea degree (cum laude) in electronic engineering from the University of Bologna, Bologna, Italy, in 1987, and the Ph.D. degree in information technology from the University of Parma, Parma, Italy, in 1994.

Since 1990, he has been with the University of Parma, where he has been a Full Professor, since 2006. His research activities have covered the study of latch-up in CMOS circuits, IC testing, modeling, characterization and reliability of power diodes and compound semiconductor and heterostructure devices, thermal modeling—particularly of GaN-based FETs, simulation of thin-film solar cells, and modeling of smart microgrids.

Open Access funding provided by 'Università degli Studi di Parma' within the CRUI CARE Agreement